plasma

MDPI

Article

Effects of Non-Thermal Electrons and Non-Extensive Positrons on Dust-Ion-Acoustic Solitary Waves in an Unmagnetized Plasma

Satyendra Nath Barman [1] and Kingkar Talukdar [2,*]

[1] Department of Mathematics, B. Borooah College, Guwahati 781007, Assam, India; snbarman.ghy@gmail.com
[2] Department of Mathematics, Gauhati University, Guwahati 781007, Assam, India
* Correspondence: kingkartalukdar5@gmail.com

Abstract

In this study, we investigated the existence and properties of solitons in an unmagnetized plasma composed of positive ions, negative ions, negatively charged dust grains, non-thermal electrons and non-extensive positrons. We have conducted our study on this complex plasma model because it moves away from simplistic and idealized plasma models. Also, a study of solitons has not previously been conducted on this complex plasma model. Through the Sagdeev potential method, we have derived the energy integral and investigated the variation in the Sagdeev potential for different values of the parameters that are involved in our plasma model. We have found that the non-thermal parameter (β) and the non-extensive parameter (q) significantly influence the features of the solitons. The features of the solitons are also found to be influenced by the Mach number (M), the negative-ion-to-positive-ion mass ratio (Ω), the positron-to-positive-ion density ratio (δ_p), the electron-to-positron temperature ratio (σ_p), the dust charge density ratio (δ_d) and the negative-ion-to-positive-ion density ratio (δ_). The results from our study can be useful in investigating plasma in astrophysical environments, such as cometary tails and interstellar clouds.

Keywords: dusty plasma; Sagdeev potential; non-thermality; non-extensive; solitary waves

1. Introduction

Unmagnetized plasma is crucial when studying astrophysical phenomena, such as solar winds, cometary tails and interstellar clouds. Several studies have been conducted on unmagnetized plasma in recent years [1–15]. The presence of dust grains can affect the soliton amplitude and Mach number for both compressive and rarefactive solitons [16]. The positive and negative solitons can significantly depend on the mass number density, ion number density, and dust polarity in the adiabatic and isothermal systems [17]. In some plasma systems, the presence of positively charged dust grains results in the existence of compressive solitons; however, the presence of negatively charged dust grains results in compressive solitons only up to a certain concentration of dust, and above the critical concentration of negative charge, the dusty plasma supports rarefactive solitons [18]. The presence of negatively charged dust particulates can result in the existence of two critical concentrations of the ion–electron density ratio [19]. The presence of dust charge of immobile dust plays a crucial role in forming compressive and rarefactive solitons in plasma, where the massive dust particles in the stationary background of the plasma and the lighter ions and relativistic electrons get appreciable initial drifts, which results in a great change in the growth of solitons [20]. The dust-ion-acoustic (DIA) solitary waves

Check for updates

Academic Editor: Andrey Starikovskiy

Received: 29 April 2026
Revised: 1 June 2026
Accepted: 6 June 2026
Published: 10 June 2026

Copyright: © 2026 by the authors. Licensee MDPI, Basel, Switzerland. This article is an open access article distributed under the terms and conditions of the Creative Commons Attribution (CC BY) license.

are highly sensitive to the ion streaming speed, and their amplitude decreases with an increase in the ion streaming speed [21]. It has also been found that the ionization instability leads to the exponential growth of the DIA solitary wave amplitude with time, whereas ion–dust and ion–neutral collisions reduce the growth rate [22]. In the presence of low dust charges and lower ion streaming, compressive and rarefactive solitons of either concave or convex character can reflect. The higher streaming of mobile dusts causes the amplitudes of rarefactive solitons to characteristically change from higher to lower, showing convex character [23]. Dust grain density enhances the amplitude of solitary waves but weakens their reflection; the amplitudes of both the incident and reflected solitons remain higher for fluctuating charge on the dust grains than in the case of fixed charge [24]. Compressive and rarefactive ion-acoustic solitary wave's characteristics significantly depend on the density and mass ratios of the positive to negative ions, the non-thermal electron parameter, and the geometry factor [25]. Large amplitude solitary structures significantly depend on various plasma parameters such as ion drift velocity, non-thermal parameter, electron to positron temperature ratio, positron density, and Mach number [26]. The presence of non-thermal electrons significantly modifies the parametric region where electron acoustic solitons can exist [27]. The non-thermal parameter significantly modify the conditions of the modulational instability of ion-acoustic waves in an electron–positron–ion plasma with nonthermal electrons [28]. The solitary excitations also strongly depend on the mass and density ratios of the positive and negative ions as well as the non-thermal electron parameter [29]. When the non-thermality of hot electrons rises, the speed of electron beam decreases, the density ratio of the beam to the cold electron increases, and the existence domain for electron acoustics solitons grows bigger [30]. The presence of non-thermal electrons also significantly affect the existence of the super solitons [31]. The presence of non-thermal electrons and protons in oxygen plasma of the ionosphere plays destructive role in the formation of electrostatic structures by nonlinear ion-acoustic waves (IAWs) [32]. Different values of the non-extensive parameter q show significant effect on chaotic motions of ion-acoustic waves [33]. The combined effects of electron non-extensivity, positron non-extensivity, and ions significantly modify the behavior of the electrostatic solitary structures that exists with positive and negative potential in some plasma models [34]. The ion-acoustic solitary wave can also depend on a non-extensive parameter, electron-to-positron temperature ratio, ion-to-electron temperature ratio and streaming velocity. Fast ion-acoustic modes solely can produce the coexistence of small-amplitude rarefactive solitons [35]. The effects of relativistic ions and q-non-extensive distribution of electrons and positrons are also crucial to the characteristics of the ion-acoustic periodic (cnoidal) wave, such as the amplitude, wavelength, and frequency [36]. The non-extensive parameter, positron-to-electron density ratio, ion-to-electron temperature ratio, electron-to-positron temperature ratio and relativistic factor can significantly influence the phase shifts of solitary waves [37]. Although, influence of non-thermal electrons and non-extensive positrons on ion-acoustic solitary waves in multi-component plasmas was investigated in [38], a study on solitons has yet not been conducted for an unmagnetized plasma model composed of positive and negative ions, negatively charged dust grains, non-thermal electrons, and non-extensive positrons. This lack of research motivates the current study.

Simultaneously incorporating Cairns non-thermal electrons and Tsallis non-extensive positrons allows the fluid model to move past the oversimplified assumption of standard thermal (Maxwellian) equilibrium. In complex, high-energy astrophysical environments, different species experience vastly different thermodynamic and kinematic constraints due to their origins and local fields. In an unmagnetized plasma, the lack of magnetic confinement allows nonlinear acoustic waves to propagate symmetrically in all directions. When the balance between plasma dispersion and nonlinearity stabilizes, it manifests

as stable solitary waves. Spacecraft like the Viking satellite and the FAST (Fast Auroral Snapshot) explorer frequently detect isolated, unmagnetized pulse-like structures known as Electrostatic Solitary Waves (ESWs) or bipolar pulses in regions where local magnetic field influences are negligible on acoustic timescales.

In this paper, we have presented the introduction in Section 1. The fluid equations (that govern our plasma model) and the standard energy integral equation are presented in Section 2. The effects of several parameters on the characteristics of solitons are discussed in Section 3. Finally, we conclude our research in Section 4.

2. Equations Governing Dynamics of Plasma

We consider an unmagnetized plasma model composed of positive and negative ions, negatively charged dust grains, non-thermal electrons and non-extensive positrons. The equations governing dynamics of plasma are as follows:

For positive ions,

$$\frac{\partial n_{i+}}{\partial t} + \frac{\partial}{\partial x}(n_{i+}u_{i+}) = 0, \tag{1}$$

$$\frac{\partial u_{i+}}{\partial t} + u_{i+}\frac{\partial u_{i+}}{\partial x} + \frac{\partial \phi}{\partial x} = 0. \tag{2}$$

For negative ions,

$$\frac{\partial n_{i-}}{\partial t} + \frac{\partial}{\partial x}(n_{i-}u_{i-}) = 0, \tag{3}$$

$$\frac{\partial u_{i-}}{\partial t} + u_{i-}\frac{\partial u_{i-}}{\partial x} - \frac{1}{\Omega}\frac{\partial \phi}{\partial x} = 0. \tag{4}$$

For negatively charged dust grains,

$$\frac{\partial n_{d-}}{\partial t} + \frac{\partial}{\partial x}(n_{d-}u_{d-}) = 0, \tag{5}$$

$$\frac{\partial u_{d-}}{\partial t} + u_{d-}\frac{\partial u_{d-}}{\partial x} = \mu_{d-}\frac{\partial \phi}{\partial x}. \tag{6}$$

Here, $\Omega = \frac{m_{i-}}{m_{i+}}$ is the negative-ion-to-positive-ion mass ratio, $\mu_{d-} = \frac{Z_{d-}m_{i+}}{m_{d-}}$ is the charge-to-mass ratio of the dust relative to the positive ions, where Z_{d-} is negative dust charge number, and m_{i+}, m_{i-} and m_{d-} are the mass of the positive ion, mass of the negative ion and mass of the negatively charged dust grain respectively. We shall consider $\mu_{d-} \ll 1$, since the negatively charged dust grains are massive as compared to ions.

We consider the following function to explain the distribution of electrons in the fast particle population [39,40]:

$$f_e(v) = \frac{n_0}{(3\alpha+1)+\sqrt{2\pi {v_e}^2}}\left(1+\frac{\alpha v^4}{{v_e}^4}\right)e^{\left(-\frac{v^2}{{v_e}^2}\right)}$$

Integrating $f_e(v)$, the non-thermal electron's number density can be obtained over velocity space with dimensionless potential ϕ as follows:

$$n_e = (1-\beta\phi+\beta\phi^2)e^{\phi} \tag{7}$$

Here, $\beta = \frac{4\alpha}{1+3\alpha}$ represents the non-thermality, where α determines the non-thermal electrons in the non-thermal plasma model. The parameter α determines the population of dynamic non-thermal electrons in the non-thermal plasma model.

The generalization of Boltzmann–Gibbs–Shannan (BGS) entropy for statistical equilibrium with long-range interactions, long-time memories, and dissipation is noted by Renyi [41] and Tsallis [42]. For two independent systems, α and β, the rule of composition

can be written as $S_q(\alpha+\beta) = S_q(\alpha) + S_q(\beta) + (1-q)S_q(\alpha)+S_q(\beta)$, $q \neq 1$ where the parameters show the grade of correlation of the system under consideration.

The non-extensive distribution function for positrons can be obtained as

$$f_p(q) = C_q\left[1-(q-1)\left(\frac{m_p u^2}{k_B T_p} + \frac{Q_p \phi}{k_B T_p}\right)\right]^{\frac{1}{q-1}}$$

where $C_q = \frac{n_{p_0}\Gamma\left(\frac{1}{1-q}\right)}{\Gamma\left(\frac{1}{1-q}-\frac{1}{2}\right)}\sqrt{\frac{m_p(1-q)}{2\pi T_p}}$, $-1 < q < 1$, and $C_q = n_{p_0}\left(\frac{1+q}{2}\right)\frac{\Gamma\left(\frac{1}{1-q}+\frac{1}{2}\right)}{\Gamma\left(\frac{1}{1-q}\right)}\sqrt{\frac{m_p(1-q)}{2\pi T_p}}$, $q > 1$.

Here, C_q is the normalization constant and Γ represents gamma function. The normalized positron number density can be given by [43]

$$n_p = \left(1-\sigma_p(q-1)\phi\right)^{\frac{q+1}{2(q-1)}} \tag{8}$$

where $\sigma_p = \frac{T_e}{T_p}$ is the electron-to-positron temperature ratio and q represents the non-extensive strength. Extensivity, sub extensivity and super extensivity are represented by q = 1, q > 1 and q < 1 respectively.

The normalized form of the Poisson equation can be obtained as

$$\frac{\partial^2\phi}{\partial x^2} = \delta_e n_e + \delta_- n_{i-} + \delta_d n_{d-} - n_{i+} - \delta_p n_p \tag{9}$$

The charge neutrality condition at equilibrium is $\delta_e + \delta_- + \delta_d = 1 + \delta_p$, where $\delta_- = \frac{n_{i-0}}{n_{i+_0}}$ is the equilibrium negative-ion-to-positive-ion density ratio, $\delta_p = \frac{n_{p_0}}{n_{i+_0}}$ is the equilibrium positron-to-positive-ion density ratio, $\delta_e = \frac{n_{e_0}}{n_{i+_0}}$ is the equilibrium electron-to-positive-ion density ratio and $\delta_d = \frac{Z_{d-}n_{d-0}}{n_{i+_0}}$ is the equilibrium dust charge density ratio.

The number densities of positive ions, negative ions, negatively charged dust grains, non-thermal electrons and non-extensive positrons are represented by n_{i+}, n_{i-}, n_{d-}, n_e and n_p respectively. The number densities are normalized by the equilibrium density of positive ion n_{i+_0}. The fluid velocities of positive ions, negative ions and negatively charged dust grains are represented by u_{i+}, u_{i-} and u_{d-} respectively, which are normalized by the ion-acoustic speed $c_s = \sqrt{\frac{k_B T_e}{m_{i+}}}$, and the electrostatic potential ϕ is normalized by $\frac{k_B T_e}{e}$, where T_e, k_B, m_{i+} and e represents electron temperature, Boltzmann's constant, positive ion mass and electronic charge respectively. The time and space variables are normalized by the inverse of the ion plasma frequency ${\omega_{pi}}^{-1} = \sqrt{\frac{m_{i+}}{4\pi e^2 n_{i+_0}}}$ and Debye length $\lambda_D = \sqrt{\frac{k_B T_e}{4\pi e^2 n_{i+_0}}}$ respectively.

We consider a variable $\xi = x - Mt$ (where M represents the Mach number) that influences all the dependent variables in the nonlinear equations to employ the Sagdeev potential (Pseudopotential) method.

Using the transformation $\xi = x - Mt$, we obtain

$$\frac{\partial}{\partial x} = \frac{\partial}{\partial \xi}\frac{\partial}{\partial x}(x-Mt) = \frac{\partial}{\partial \xi} \text{ and } \frac{\partial}{\partial t} = \frac{\partial}{\partial \xi}\frac{\partial}{\partial t}(x-Mt) = -M\frac{\partial}{\partial \xi}$$

Applying the boundary conditions $\xi \to \pm\infty$, $n_{i+} \to 1$, $n_{i-} \to 1$, $n_{d-} \to 1$ $u_{i+} \to 0$, $u_{i-} \to 0$, $u_{d-} \to 0$, $\phi \to 0$, we obtain the overall solution for n_{i+}, n_{i-} and n_{d-} as the following respectively:

$$n_{i+} = \left(1 - \frac{2\phi}{M^2}\right)^{-\frac{1}{2}} \tag{10}$$

$$n_{i-} = \left(1 + \frac{2\phi}{\Omega M^2}\right)^{-\frac{1}{2}} \tag{11}$$

$$n_{d-} = \left(1 + \frac{2\mu_{d-}\phi}{M^2}\right)^{-\frac{1}{2}} \tag{12}$$

Applying the fundamental densities from the Equations (7), (8) and (10)–(12) into the Equation (9), we obtain

$$\frac{\partial^2\phi}{\partial\xi^2} = \delta_e(1 - \beta\phi + \beta\phi^2)e^{\Phi} + \delta_-\left(1 + \frac{2\phi}{\Omega M^2}\right)^{-\frac{1}{2}} + \delta_d\left(1 + \frac{2\mu_{d-}\phi}{M^2}\right)^{-\frac{1}{2}} - \left(1 - \frac{2\phi}{M^2}\right)^{-\frac{1}{2}} - \delta_p\left(1 - \sigma_p(q-1)\phi\right)^{\frac{q+1}{2(q-1)}}$$

Now, multiplying $\frac{d\phi}{d\xi}$ in the above equation and then integrating, we obtain the standard energy integral equation:

$$\frac{1}{2}\left(\frac{d\phi}{d\xi}\right)^2 + V(\phi) = 0 \tag{13}$$

Here, $V(\phi)$ denotes the Sagdeev potential in the energy integral equation (13). The $V(\phi)$ is given by

$$\begin{aligned} V(\phi) = &-\frac{\delta_d M^2}{\mu_{d-}}\left(\sqrt{1 + \frac{2\mu_{d-}\phi}{M^2}} - 1\right) - \Omega\delta_- M^2\left(\sqrt{1 + \frac{2\phi}{M^2\Omega}} - 1\right) - M^2\left(\sqrt{1 - \frac{2\phi}{M^2}} - 1\right) \\ &-\delta_e\left(\left(1 + 3\beta - 3\beta\phi + \beta\phi^2\right)e^{\Phi} - (1 + 3\beta)\right) - \frac{2\delta_p}{\sigma_p(3q-1)}\left(\left(1 - (q-1)\sigma_p\phi\right)^{\frac{3q-1}{2(q-1)}} - 1\right) \end{aligned} \tag{14}$$

To guarantee the structural existence and physical stability of localized electrostatic solitary wave solutions, the self-consistent Sagdeev pseudopotential $V(\phi)$ must rigorously satisfy a system of four core mathematical boundary conditions. First, the pseudopotential curve must pass precisely through the unperturbed origin, yielding $V(\phi) = 0$ at $\phi = 0$. Second, the net pseudo-force must vanish at this baseline boundary, satisfying the equilibrium condition $\frac{dV(\phi)}{d\phi} = 0$ at $\phi = 0$. Third, for localized acoustic pulses to safely form, the origin must behave as a local potential maximum (an unstable fixed point), which strictly dictates that the second derivative must be negative: i.e., $\frac{d^2V(\phi)}{d\phi^2} < 0$ at $\phi = 0$. This specific inequality analytically establishes the lower threshold constraint for the minimum Mach number ($M > M_{min}$). Finally, a real bounding turning point ϕ_m must exist where the profile intersects the axis again such that $V(\phi_m) = 0$, while maintaining a net restorative force. Consequently, stable solitary profiles are physically viable if and only if the pseudopotential remains strictly negative ($V(\phi) < 0$) throughout the entire localized domain spanning $0 < \phi < \phi_m$ for compressive solitons, or $\phi_m < \phi < 0$ for rarefactive solitons.

The condition $\frac{d^2V(\phi)}{d\phi^2} < 0$ at $\phi = 0$ gives the lower limit of Mach number (M_{min}) as

$$M_{min} = \sqrt{\frac{2(\delta_- + \Omega + \delta_d\mu_{d-}\Omega)}{2\delta_e\Omega(1-\beta) + \Omega\delta_p\sigma_p(q+1)}}$$

From Equation (10) we observe that for n_{i+} to be real we must have $M^2 \geq 2\phi$. Thus, the extreme value of ϕ is

$$\phi_m = \phi_0 = \frac{M^2}{2} \tag{15}$$

Substituting the extreme value of ϕ from Equation (15) in (14) we get the M upper limit as $V(\phi) \geq 0$, which gives

$$-\delta_e\left[\left(1+3\beta-\tfrac{3}{2}\beta M^2+\tfrac{1}{4}\beta M^4\right)e^{\frac{M^2}{2}}-(1+3\beta)\right]-\Omega\delta_- M^2\left[\sqrt{1+\tfrac{1}{\Omega}}-1\right]+M^2$$
$$-\frac{2\delta_p}{\sigma_p(3q-1)}\left[\left(1-(q-1)\sigma_p\frac{M^2}{2}\right)^{\frac{3q-1}{2(q-1)}}-1\right]-\frac{\delta_d M^2}{\mu_{d-}}\left[\sqrt{1+\mu_{d-}}-1\right]\geq 0$$

It is also crucial to investigate the profiles of solitary waves when their amplitudes are no longer arbitrary but small. To study small-amplitude solitary waves, the Sagdeev potential V(φ) can be Taylor expanded about φ = 0 up to a reasonable order of φ so as to obtain a soliton solution from the energy integral equation.

Therefore, Equation (13) can be reduced to

$$\frac{1}{2}\left(\frac{d\phi}{d\xi}\right)^2+A\phi^2+B\phi^3=0 \tag{16}$$

where $A=\frac{\beta\delta_e}{2}-\frac{\delta_e}{2}+\frac{1}{2M^2}+\frac{\delta_-}{2M^2\Omega}-\frac{\delta_p\sigma_p(q+1)}{4}+\frac{\delta_d\mu_{d-}}{2M^2}$,

$$B=-\frac{\delta_e}{6}+\frac{1}{2M^4}-\frac{\delta_-}{2M^4\Omega^2}+\frac{\delta_p(q+1)(q-3){\sigma_p}^2}{24}-\frac{\delta_d{\mu_{d-}}^2}{2M^4}$$

Integrating Equation (16) and using the boundary conditions stated before, we obtain the soliton solution as

$$\phi=\phi_m sech^2\left(\frac{\xi}{w}\right)$$

where $\phi_m=-\frac{A}{B}$ and $w=\sqrt{-\frac{2}{A}}$ represents the amplitude and width of soliton respectively.

3. Results and Discussion

The existence, structure, and characteristics of large-amplitude nonlinear waves, particularly solitary waves, can be analyzed by using the Sagdeev potential method. In this section of the paper, we investigate the variation in the Sagdeev potential for different values of the plasma parameters.

Figure 1 shows the variation in the Sagdeev potential for different values of q and fixed δ_e = 0.7, β = 0.15, Ω = 1, δ_- = 0.18, M = 1.4, $\mu_{d_}$ = 0.0000778, δ_d = 0.67, δ_p = 0.55, and σ_p = 0.3. We can observe that, as the non-extensive parameter (q) increases, the depth of the Sagdeev potential well increases. A higher value of q indicates a distribution that is more concentrated at lower energies and the positrons respond more strongly to the wave's electric field. This strengthens the nonlinearity of the plasma, allowing it to support taller and more robust solitary pulses, which corresponds to a deeper Sagdeev potential well. Figure 2 shows the variation in the Sagdeev potential for different values of M and fixed δ_e = 0.7, β = 0.15, Ω = 1, δ_- = 0.18, $\mu_{d_}$ = 0.0000778, δ_d = 0.67, δ_p = 0.55, σ_p = 0.3, and q = 0.6. We can observe that, as the Mach number (M) increases, the depth of the Sagdeev potential well increases. A higher Mach number corresponds to a faster, more energetic solitary wave. To sustain such a wave, the plasma creates a stronger electrostatic trench (deeper potential well) to keep the particles trapped in the solitary structure.

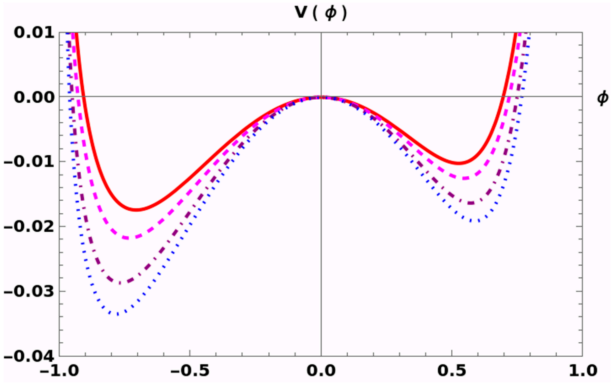


Figure 1. Variation in Sagdeev potential V(ϕ) with respect to ϕ for q = 0.6 (solid line), 0.8 (dashed line), 1.1 (dot-dashed line), 1.3 (dotted line).

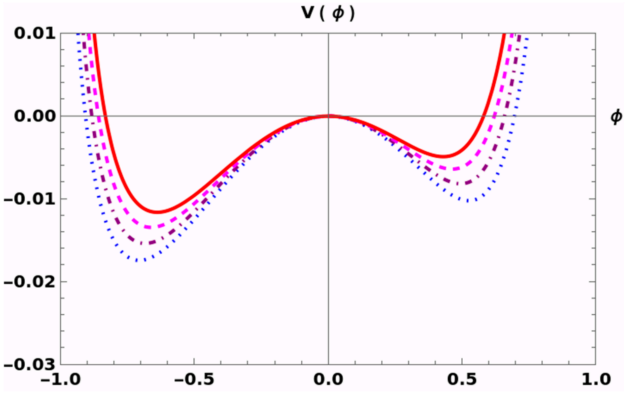


Figure 2. Variation in Sagdeev potential V(ϕ) with respect to ϕ for M = 1.37 (solid line), 1.38 (Dashed line), 1.39 (dot-dashed line), 1.4 (dotted line).

Figure 3 shows the variation in the Sagdeev potential for different values of β and fixed δ_e = 0.7, Ω = 1, δ_- = 0.18, M = 1.4, $\mu_{d_}$ = 0.0000778, δ_d = 0.67, δ_p = 0.55, σ_p = 0.3, and q = 0.6. We can observe that, as the non-thermal parameter (β) increases, the depth of the Sagdeev potential well decreases. Therefore, the non-thermal parameter significantly modifies the balance between nonlinear steepening and wave dispersion. The extra energy from non-thermal electrons acts to suppress the growth of large-amplitude solitary waves. Figure 4 shows the variation in the Sagdeev potential for different values of σ_p and fixed δ_e = 0.7, β = 0.15, Ω = 1, δ_- = 0.18, M = 1.4, $\mu_{d_}$ = 0.0000778, δ_d = 0.67, δ_p = 0.55, and q = 0.6. We can observe that, as the electron to positron temperature ratio (σ_p) increases, the depth of the Sagdeev potential well increases. Therefore, as σ_p increases, positrons become colder relative to electrons, and the nonlinearity of the plasma system increases while the dispersion decreases. This shifts the balance towards more robust nonlinear structures, allowing the potential well to extend to greater depths.

Figure 5 shows the variation in the Sagdeev potential for different values of δ_p and fixed β = 0.1, Ω = 1, δ_- = 0.18, M = 1.4, $\mu_{d_}$ = 0.0000778, δ_d = 0.67, σ_p = 0.3, and q = 0.6. We can observe that, as the positron-to-positive-ion density ratio (δ_p) increases, the depth of the Sagdeev potential well increases. Therefore, when positrons follow a non-extensive (q-distributed) distribution, the system becomes more sensitive to density changes. The non-extensivity parameter (q) amplifies the effects of adding positrons, further deepening the potential well. Figure 6 shows the variation in the Sagdeev potential for different values of δ_- and fixed β = 0.1, Ω = 1, M = 1.4, $\mu_{d_}$ = 0.0000778, δ_d = 0.67, δ_p = 0.55, σ_p = 0.3, and q = 0.6. We can observe that, as the negative-ion-to-positive-ion density ratio (δ_-) increases, the depth of the Sagdeev potential well decreases. Therefore, as the density of negative ions

increases, they compete with electrons to balance the charge of the positive ions. Electrons are highly mobile and shield potentials effectively as compared to negative ions that are heavy and sluggish. The shift in the population from the electrons to the negative ions modifies the Debye shielding length. This modification restricts the maximum electrostatic pulse height that the plasma can support before the wave breaks, leading to a shallower potential well.

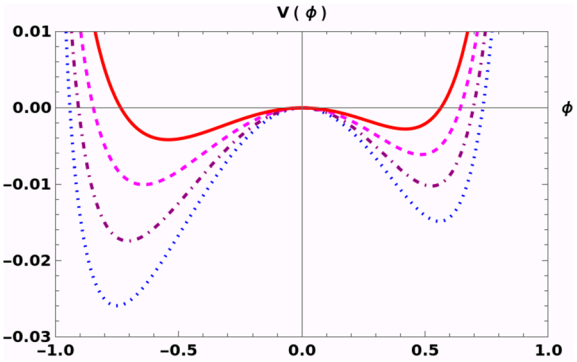


Figure 3. Variation in Sagdeev potential V(ϕ) with respect to ϕ for β = 0.25 (solid line), 0.20 (dashed line), 0.15 (dot-dashed line), 0.10 (dotted line).

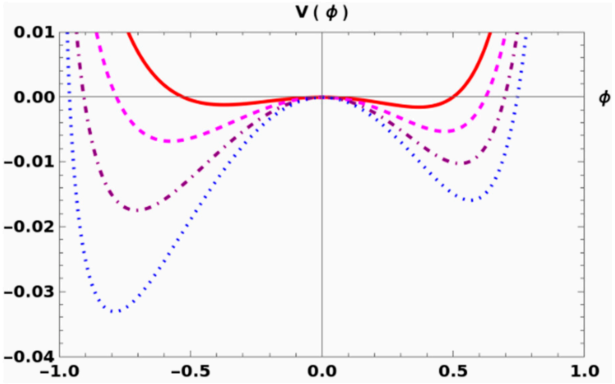


Figure 4. Variation in Sagdeev potential V(ϕ) with respect to ϕ for σ_p = 0.1 (solid line), 0.2 (dashed line), 0.3 (dot-dashed line), 0.4 (dotted line).

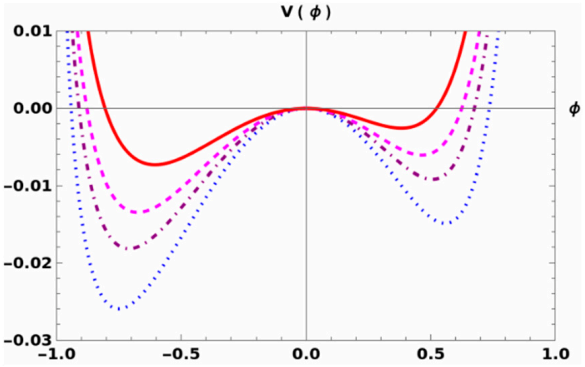


Figure 5. Variation in Sagdeev potential V(ϕ) with respect to ϕ for δ_p = 0.47 (solid line), 0.50 (dashed line), 0.52 (dot-dashed line), 0.55 (dotted line).

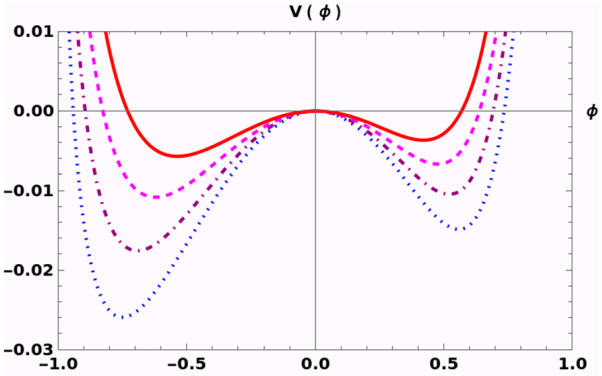


Figure 6. Variation in Sagdeev potential V(ϕ) with respect to ϕ for δ_{-} = 0.24 (solid line), 0.22 (dashed line), 0.20 (dot-dashed line), 0.18 (dotted line).

Figure 7 shows the variation in the Sagdeev potential for different values of δ_d and fixed $\beta = 0.1$, $\Omega = 1$, $\delta_{-} = 0.18$, $M = 1.4$, $\mu_{d_{-}} = 0.0000778$, $\delta_p = 0.55$, $\sigma_p = 0.3$, and $q = 0.6$. We can observe that, as the dust charge density ratio (δ_d) increases, the depth of the Sagdeev potential well decreases. The dust grains reduce the effective electron density and dampen the nonlinear restoring forces required to sustain large-amplitude solitary waves. This causes a decrease in the depth of the Sagdeev potential well with an increasing dust charge density ratio. Figure 8 shows the variation in the Sagdeev potential for different values of Ω and fixed $\delta_e = 0.7$, $\beta = 0.15$, $\delta_{-} = 0.18$, $M = 1.39$, $\mu_{d_{-}} = 0.0000778$, $\delta_d = 0.67$, $\delta_p = 0.55$, $\sigma_p = 0.1$, and $q = 0.6$. We can observe that, as the negative-ion-to-positive-ion mass ratio (Ω) increases, the depth of the Sagdeev potential well increases. As the negative ions become heavier, they become harder to move and carry more momentum. Therefore, to successfully govern their motion and maintain a stable soliton structure, the plasma generates a deeper Sagdeev potential well.

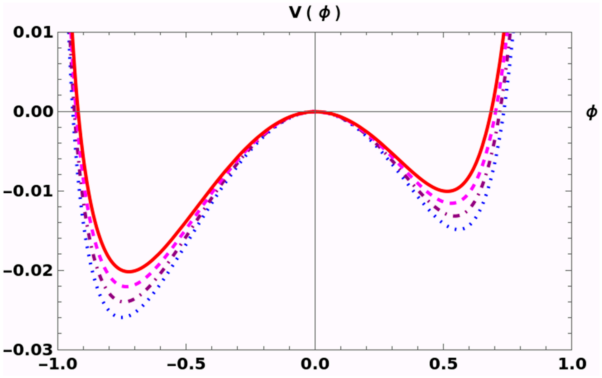


Figure 7. Variation in Sagdeev potential V(ϕ) with respect to ϕ for δ_d = 0.70 (solid line), 0.69 (dashed line), 0.68 (dot-dashed line), 0.68 (dotted line).

The analytical tractability of our present five-component plasma model relies on three standard physical approximations, which align well with the observed cosmic regimes. First, the unmagnetized plasma assumption is justified because the characteristic soliton frequency strictly dominates the heavy particle gyrofrequencies, rendering magnetic Lorentz forces negligible. Second, the equilibrium charge neutrality condition is robustly maintained across the macroscopic spatial dimensions of interstellar clouds, where localized micro-fields are rapidly shielded out. Finally, given that the dust-to-ion mass ratio is exceptionally large, the parameter $\mu_{d_{-}} \ll 1$ ensures that the massive dust grains remain practically stationary on the fast timescales of the ion-acoustic solitary structures. Conse-

quently, these constraints perfectly isolate the pure acoustic nonlinearities without loss of physical generality.

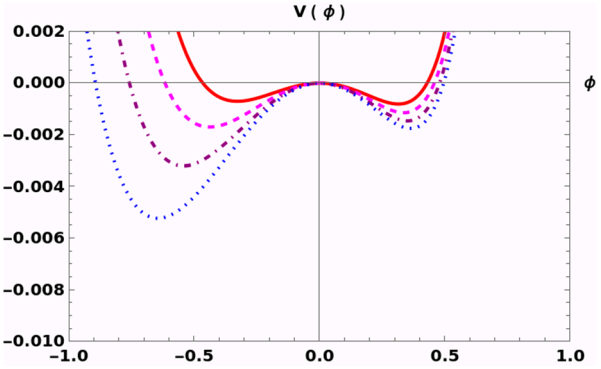


Figure 8. Variation in Sagdeev potential V(ϕ) with respect to ϕ for $\Omega = 1.0$ (solid line), 1.1 (dashed line), 1.2 (dot-dashed line), 1.3 (dotted line).

To validate the generalized nature of the current model, we consider the classical thermal limit where the non-thermal parameter vanishes $\beta \to 0$ and the non-extensive index approaches unity $q \to 1$. In this thermodynamic limit, the Cairns electron distribution (Equation (7)) and Tsallis positron distribution (Equation (8)) collapse exactly into the classical Maxwellian profiles, where $n_e \to e^{\phi}$ and $n_p \to e^{-\sigma_p \phi}$. Physically, removing the high-energy particle tails restores standard Debye shielding across the plasma matrix. Consequently, the Sagdeev potential well becomes shallower, leading to a noticeable reduction in both the amplitude and energy of the compressive and rarefactive solitons compared to the non-equilibrium regimes. This baseline reduction confirms that non-thermal and non-extensive environments are fundamentally responsible for supporting highly energetic, elevated solitary wave profiles.

The physical stability of the predicted compressive and rarefactive solitary waves is fundamentally governed by a self-consistent balance between convective hydrodynamic steepening and localized plasma dispersion. Mathematically, stable soliton propagation requires the Sagdeev pseudo-potential $V(\phi)$ to form a valid, closed potential well satisfying $\frac{d^2V(\phi)}{d\phi^2} < 0$ at the origin, which restricts solutions to a specific supersonic window $M > M_{min} > 1$. We have found $M_{min} = 1.017$ for $\beta = 0.25$ (Figure 3). At a microscopic level, the non-equilibrium populations further reinforce this stability; the fast, super-thermal particles governed by the non-extensive and non-thermal distributions rapidly redistribute in response to localized field fluctuations. This rapid kinetic shielding prevents wave filamentation, ensuring that the solitary structures remain structurally stable against small-scale spatial perturbations.

To establish the quantitative relevance of our selected parameter ranges, we map our fluid model directly onto measured space plasma criteria [44,45]. In cometary environments, such as the plasma tail of Comet Halley scrutinized by the Giotto mission, the background density $n_{i+_0} \sim$10–100 cm^{-3} and solar wind-driven electron acceleration correspond to non-thermal parameters of $\beta \approx 0.1$–0.3 and the dust charge fractions of $\delta_d \approx 0.1$–0.4. Furthermore, in diffuse interstellar clouds, cosmic ray-induced electron–positron pair production amidst oxygen cluster ions yields a mass ratio of $\Omega \approx 1.0$. The localized density structures recorded in these environments travel as pure acoustic pulses at Mach numbers of $1.05 \leq M \leq 1.4$. This close numerical agreement demonstrates that our selected non-extensive and non-thermal windows $0.6 \leq q \leq 1.3$ and $0 \leq \beta \leq 0.5$ capture physically real, observable space conditions rather than isolated mathematical regimes.

From Figures 9–14, we can observe that the amplitude of solitons increases for increasing values of q and δ_e; however, the amplitude of solitons decreases for increasing values of β and δ_d. Therefore, the propagation of soliton in both the arbitrary and small-amplitude profile are identical for our considered plasma model.

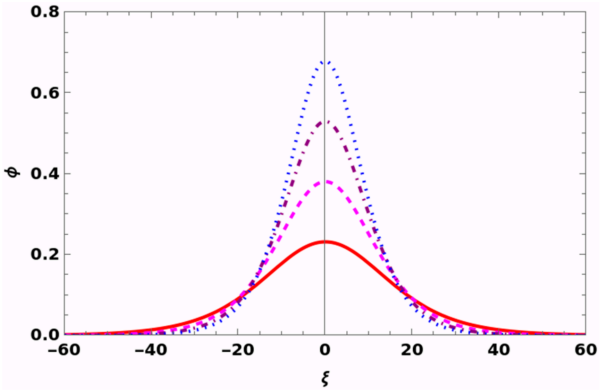


Figure 9. Compressive soliton profile for $\beta = 0.16$ (solid line), 0.15 (dashed line), 0.14 (dot-dashed line), 0.13 (dotted line) and fixed $\delta_e = 0.7$, $\delta_- = 0.18$, $\Omega = 1$, $\delta_p = 0.55$, $\sigma_p = 0.3$, $\delta_d = 0.67$, $\mu_{d-} = 0.0000778$, $M = 1.29$, and $q = 0.6$.

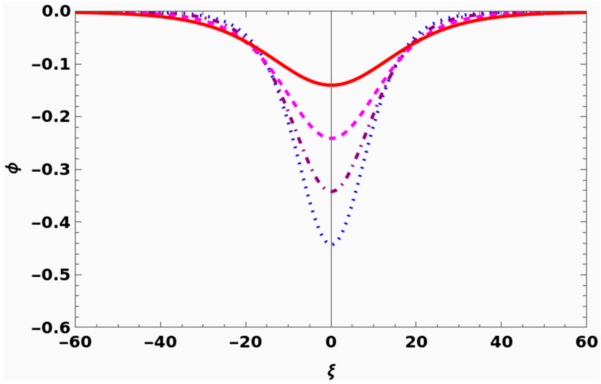


Figure 10. Rarefactive soliton profile for $\beta = 0.13$ (solid line), 0.12 (dashed line), 0.11 (dot-dashed line), 0.10 (dotted line) and fixed $\delta_e = 0.75$, $\delta_- = 0.42$, $\Omega = 1$, $\delta_p = 0.66$, $\sigma_p = 0.4$, $\delta_d = 0.61$, $\mu_{d-} = 0.0000778$, $M = 1.29$, and $q = 0.6$.

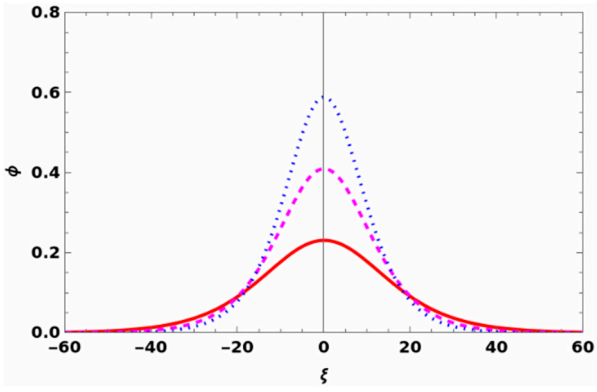


Figure 11. Compressive soliton profile for $q = 0.6$ (solid line), 0.7 (dashed line), 0.8 (dotted line) and fixed $\delta_e = 0.7$, $\beta = 0.16$, $\delta_- = 0.18$, $\Omega = 1$, $\delta_p = 0.55$, $\sigma_p = 0.3$, $\delta_d = 0.67$, $\mu_{d-} = 0.0000778$, and $M = 1.29$.

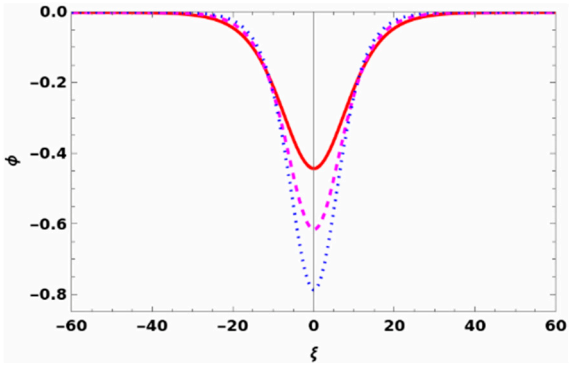


Figure 12. Rarefactive soliton profile for q = 0.6 (solid line), 0.7 (dashed line), 0.8 (dotted line) and fixed δ_e = 0.75, β = 0.1, δ_ = 0.42, Ω = 1, δ_p = 0.66, σ_p = 0.4, δ_d = 0.61, μ_{d-} = 0.0000778, and M = 1.29.

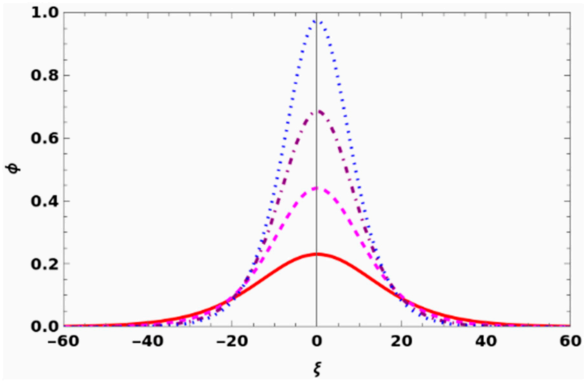


Figure 13. Compressive soliton profile for δ_d = 0.67 (solid), 0.66 (dashed line), 0.65 (dot-dashed line), 0.64 (dotted line) and fixed δ_e = 0.7, β = 0.16, δ_ = 0.18, Ω = 1, δ_p = 0.55, σ_p = 0.3, μ_{d-} = 0.0000778, M = 1.29, and q = 0.6.

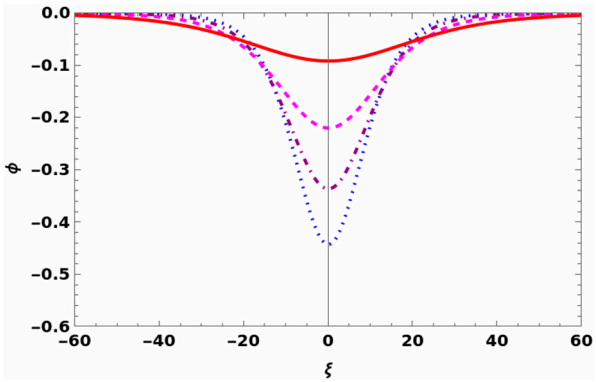


Figure 14. Rarefactive soliton profile for δ_e = 0.72 (solid line), 0.73 (dashed line), 0.74 (dot-dashed line), 0.75 (dotted line) and fixed δ_e = 0.75, β = 0.1, δ_ = 0.42, Ω = 1, δ_p = 0.66, σ_p = 0.4, δ_d = 0.61, μ_{d-} = 0.0000778, M = 1.29, and q = 0.6.

4. Conclusions

In the study of an unmagnetized plasma composed of positive ions, negative ions, negatively charged dust grains, non-thermal electrons and non-extensive positrons, we have found the existence of both the compressive and rarefactive solitons. An increase in the depth of the Sagdeev potential well represents an increase in the energy and amplitude of the solitons. The amplitude of the rarefactive solitons is found to be comparatively higher than that the compressive solitons. The amplitudes of both the compressive and rarefactive solitons are found to be decreased for increasing value of the non-thermal parameter (β); however, the amplitudes of both the compressive and rarefactive solitons are found to be

increased for increasing value of the non-extensive parameter (q). Also, an increase in the Mach number (M), the negative-ion-to-positive-ion mass ratio (Ω), the positron-to-positive ion density ratio (δ_p) and the electron-to-positron temperature ratio (σ_p) increases the amplitude of both the compressive and rarefactive solitons; however, an increase in the dust charge density ratio (δ_d) and the negative-ion-to-positive-ion density ratio (δ_) decreases the amplitude of both the compressive and rarefactive solitons. Solitons are found to exist for $0.6 \leq q \leq 1.3$ (q < 1 and q > 1 represents super extensivity and sub extensivity respectively). Solar wind electron/ion data from the Wind and Ulysses spacecraft regularly yield q values between 0.7 and 1.1. Non-neutral plasma traps tracking long-range transport confirm $q \neq 1$ behaviors in this exact mathematical window. In laboratory laser-induced fusion setups, strong localized electric fields instantly accelerate a faction of electrons, matching these exact non-thermal profiles. Also, double-plasma devices generating localized ion-acoustic solitons explicitly measure stable solitary wave propagation in the range of $1.1 \leq M \leq 1.6$. In astrophysical environments, positrons generated via high-energy pair production cool down rapidly through synchrotron radiation, making them significantly colder than the background electrons. The non-extensive parameter (q) physically measures the degree of non-locality and long-range correlation within the positron distribution, moving beyond the classical Boltzmann–Gibbs framework $(q = 1)$. Microscopically, values of $(0.6 \leq q < 1)$ correspond to a super-extensive state characterized by a high-energy power law tail of fast positrons. Conversely, $1 < q \leq 1.3$ indicates a sub-extensive regime exhibiting a strict high-velocity thermal cutoff. As q increases within the valid domain, the shift in the positron thermal pressure significantly alters the plasma's Debye shielding capacity. This micro-structural modification directly enhances the self-consistent electrostatic restoring force, providing the physical mechanism behind the observed increase in both compressive and rarefactive soliton amplitudes.

Author Contributions: Conceptualization, S.N.B. and K.T. Software, Wolfram Mathematica Investigation, S.N.B. and K.T. Writing-original draft preparation, S.N.B. and K.T. Supervision, S.N.B. All authors have read and agreed to the published version of the manuscript.

Funding: The authors have not received any financial support for this research.

Data Availability Statement: All data underlying the results are available as part of the article and no additional source data are required.

Conflicts of Interest: The authors declare no conflict of interests.

References

1. Mandal, P.; Maji, T.K.; Samanta, U.K.; Ghorui, M.K. Head-on collision of ion-acoustic KP solitons in unmagnetized e-p-i plasma. *Indian J. Phys.* **2025**, *99*, 4833–4843. [CrossRef]
2. Moinuddin, A.S.M.; Alam, M.S.; Talukder, M.R. Head-on collision of ion-acoustic waves in multi-component unmagnetized plasmas. *Waves Random Complex Media* **2022**, *32*, 2657–2676. [CrossRef]
3. Imon, U.; Alam, M.S. Consequence of head-on collision of ion acoustic waves in unmagnetized plasmas having generalized (*r*, *q*) distributed electrons and positrons. *Waves Random Complex Media* **2023**, 1–28. [CrossRef]
4. Halder, P.; Bandyopadhyay, A.; Sardar, S. Arbitrary Amplitude Dust–Ion Acoustic Solitary Structures in Five Components Unmagnetized Plasma. *Plasma Phys. Rep.* **2023**, *49*, 467–483. [CrossRef]
5. Dubinov, A.E.; Kolotkov, D.Y. Ion-acoustic supersolitons in plasma. *Plasma Phys. Rep.* **2012**, *38*, 909–912. [CrossRef]
6. Rahman, O.; Hafez, M.G.; Barua, S.; Kauser, M.A. Ion acoustic solitons and periodic waves with dynamical features around the supercritical values in relativistic unmagnetized plasmas. *Phys. Scr.* **2025**, *100*, 025201. [CrossRef]
7. Lakhina, G.S.; Kakad, A.P.; Singh, S.V.; Verheest, F. Ion- and electron-acoustic solitons in two-electron temperature space plasmas. *Phys. Plasmas* **2008**, *15*, 062903. [CrossRef]
8. Hafez, M.G.; Talukder, M.R. Ion acoustic solitary waves in plasmas with nonextensive electrons, Boltzmann positrons and relativistic thermal ions. *Astrophys. Space Sci.* **2015**, *359*, 27. [CrossRef]

9. Islam, M.N.; Hafez, M.G.; Deb, U.K. Heavy Ion-Acoustic Soliton and Dressed Soliton in an Unmagnetized Weakly and Strongly Coupled Plasma. *Braz. J. Phys.* **2022**, *52*, 158. [CrossRef]
10. Hafez, M.G.; Talukder, M.R.; Ali, M.H. Nonlinear propagation of weakly relativistic ion-acoustic waves in electron–positron–ion plasma. *Pramana* **2016**, *87*, 70. [CrossRef]
11. Ur-Rehman, H.; Mahmood, S. Higher order contribution to ion-acoustic Korteweg–de Vries (KdV) soliton in unmagnetized quantum plasmas with arbitrary degeneracy of electrons. *Phys. Scr.* **2024**, *99*, 075608. [CrossRef]
12. Alinejad, H. Non-linear localized ion-acoustic waves in electron–positron–ion plasmas with trapped and non-thermal electrons. *Astrophys. Space Sci.* **2010**, *325*, 209–215. [CrossRef]
13. Hafez, M.G.; Talukder, M.R.; Sakthivel, R. Ion acoustic solitary waves in plasmas with nonextensive distributed electrons, positrons and relativistic thermal ions. *Indian J. Phys.* **2016**, *90*, 603–611. [CrossRef]
14. Kaladze, T.; Mahmood, S.; Ur-Rehman, H. Acoustic nonlinear periodic (cnoidal) waves and solitons in pair-ion plasmas. *Phys. Scr.* **2012**, *86*, 035506. [CrossRef]
15. Dalui, S.; Bandyopadhyay, A. Effect of Landau damping on ion acoustic solitary waves in a collisionless unmagnetized plasma consisting of nonthermal and isothermal electrons. *Indian J. Phys.* **2021**, *95*, 367–381. [CrossRef]
16. Bharuthram, R.; Shukla, P. Large amplitude ion-acoustic solitons in a dusty plasma. *Planet. Space Sci.* **1992**, *40*, 973–977. [CrossRef]
17. Islam, K.A.; Deeba, F.; Hassan, K.A. Dust ion acoustic solitons in a complex dusty plasma system with an adiabatic state. *Heliyon* **2020**, *6*, e05373. [CrossRef] [PubMed]
18. Tiwari, R.S.; Mishra, M.K. Ion-acoustic dressed solitons in a dusty plasma. *Phys. Plasmas* **2006**, *13*, 062112. [CrossRef]
19. Ghosh, S.; Bharuthram, R. Ion acoustic solitons and double layers in electron–positron–ion plasmas with dust particulates. *Astrophys. Space Sci.* **2008**, *314*, 121–127. [CrossRef]
20. Das, S. Weak Relativistic Effect in the Formation of Ion-Acoustic Solitary Waves in Dusty Plasma. *IEEE Trans. Plasma Sci.* **2022**, *50*, 2225–2229. [CrossRef]
21. Shahmansouri, M.; Tribeche, M. Large amplitude dust ion acoustic solitons and double layers in dusty plasmas with ion streaming and high-energy tail electron distribution. *Commun. Theor. Phys.* **2014**, *61*, 377. [CrossRef]
22. Ghosh, S. Effect of ionization on ion acoustic solitary waves in a collisional dusty plasma. *J. Plasma Phys.* **2005**, *71*, 519–526. [CrossRef]
23. Das, S. Propagation of dust ion acoustic solitary waves in dusty plasma with Boltzmann electrons. *J. Phys. Conf. Ser.* **2019**, *1290*, 012025. [CrossRef]
24. Tomar, R.; Malik, H.K.; Dahiya, R.P. Reflection of ion acoustic solitary waves in a dusty plasma with variable charge dust. *J. Theor. Appl. Phys.* **2014**, *8*, 126. [CrossRef]
25. Selim, M.M. Spherical ion acoustic waves in pair ion plasmas with nonthermal electrons. *Eur. Phys. J. Plus* **2016**, *131*, 93. [CrossRef]
26. Das, M.; Madhukalya, B.; Das, R. Ion acoustic solitary waves in multicomponent plasmas: Influence of ion drift velocity and nonthermal electrons. *Heat Transf.* **2024**, *53*, 2062–2072. [CrossRef]
27. Singh, S.V.; Lakhina, G.S. Electron acoustic solitary waves with non-thermal distribution of electrons. *Nonlinear Process. Geophys.* **2004**, *11*, 275–279. [CrossRef]
28. Gill, T.S.; Bains, A.S.; Saini, N.S.; Bedi, C. Ion-acoustic envelope excitations in electron–positron–ion plasma with nonthermal electrons. *Phys. Lett. A* **2010**, *374*, 3210–3215. [CrossRef]
29. Sabry, R.; Moslem, W.M.; Shukla, P.K. Fully nonlinear ion-acoustic solitary waves in a plasma with positive-negative ions and nonthermal electrons. *Phys. Plasmas* **2009**, *16*, 032302. [CrossRef]
30. Alyousef, H.A.; Naeem, S.N.; Irshad, M.; Rahman, A.U.; Ismaeel, S.M.E.; El-Tantawy, S.A. The impact of electron beams on the arbitrary amplitude electron–acoustic solitons in a nonthermal plasma. *Phys. Fluids* **2024**, *36*, 015139. [CrossRef]
31. Singh, S.; Lakhina, G. Ion-acoustic supersolitons in the presence of non-thermal electrons. *Commun. Nonlinear Sci. Numer. Simul.* **2015**, *23*, 274–281. [CrossRef]
32. Shan, S.A.; Hassan, I.; Saleem, H. Electrostatic wave instability and soliton formation with non-thermal electrons in O-H plasma of ionosphere. *Phys. Plasmas* **2019**, *26*, 022114. [CrossRef]
33. Ghosh, U.N.; Saha, A.; Pal, N.; Chatterjee, P. Dynamic structures of nonlinear ion acoustic waves in a nonextensive electron–positron–ion plasma. *J. Theor. Appl. Phys.* **2015**, *9*, 321–329. [CrossRef]
34. Ferdousi, M.; Yasmin, S.; Ashraf, S.; Mamun, A.A. Nonlinear propagation of ion-acoustic waves in an electron-positron-ion plasma. *Astrophys. Space Sci.* **2014**, *352*, 579–584. [CrossRef]
35. Khanam, R.; Barman, S.N. The Formation of Ion-Acoustic Solitary Waves in a Plasma Having Nonextensive Electrons and Positrons. *East Eur. J. Phys.* **2024**, *4*, 518–525. [CrossRef]
36. Farhadkiyaei, F. Ion acoustic cnoidal waves in electron-positron-ion plasmas with q-nonextensive electrons and positrons and high relativistic ions. *J. Theor. Appl. Phys.* **2023**, *17*. [CrossRef]
37. Khaled, M.A. On the head-on collision between two ion acoustic solitary waves in a weakly relativistic plasma containing nonextensive electrons and positrons. *Astrophys. Space Sci.* **2014**, *350*, 607–614. [CrossRef]

38. Nasir, M.; Ameen, L.; Asghar, B.; Rani, A.; Beemkumar, N.; Jain, V.; Imtiaz, S.; Ullah, M.F.; Hejazi, H.A.; Mohammed, N.A.; et al. Influence of non-thermal electrons and non-extensive positrons on ion acoustic solitary waves in multi-component plasmas. *Int. Commun. Heat Mass Transf.* **2026**, *170*, 110026. [CrossRef]
39. Rényi, A. On a new axiomatic theory of probability. *Acta Math. Hung.* **1955**, *6*, 285–335. [CrossRef]
40. Tsallis, C. Possible generalization of Boltzmann-Gibbs statistics. *J. Stat. Phys.* **1988**, *52*, 479–487. [CrossRef]
41. Khattak, M.N.; Mushtaq, A.; Ehsan, Z. Electrostatic baryonic solitary waves in ambiplasma with nonextensive leptons. *Chin. J. Phys.* **2016**, *54*, 503–514. [CrossRef]
42. Ghosh, S.; May, M.J.; Kopp, E.B. NF-κB and Rel proteins: Evolutionarily conserved mediators of immune responses. *Annu. Rev. Immun.* **1998**, *16*, 225–260. [CrossRef] [PubMed]
43. Verheest, F.; Pillay, S.R. Large amplitude dust-acoustic solitary waves and double layers in nonthermal plasmas. *Phys. Plasmas* **2008**, *15*, 013703. [CrossRef]
44. Vineeth, S.; Prabhakar, S.; Sebastian, S.; Abraham, N.P. Solitary waves in a cometary plasma with heavy dust ion pairs. *Phys. Plasmas* **2021**, *28*, 033701. [CrossRef]
45. Tarofder, S.; Mannan, A.; Mamun, A. Solitary wave solution of (3 + 1)-dimensional cylindrical Kadomstev–Petviashvili equation in warm opposite polarity dusty plasma. *Results Phys.* **2023**, *49*, 106530. [CrossRef]

Disclaimer/Publisher's Note: The statements, opinions and data contained in all publications are solely those of the individual author(s) and contributor(s) and not of MDPI and/or the editor(s). MDPI and/or the editor(s) disclaim responsibility for any injury to people or property resulting from any ideas, methods, instructions or products referred to in the content.